

Hierarchical Spherical Harmonics Based Deformable HARDI Registration

Pew-Thian Yap¹, Yasheng Chen¹, Hongyu An¹, John H. Gilmore²,
Weili Lin¹, and Dinggang Shen¹

¹ BRIC, Department of Radiology and

² Department of Pyschiatry

University of North Carolina at Chapel Hill, NC

Abstract. In contrast to the more common Diffusion Tensor Imaging (DTI), High Angular Resolution Diffusion Imaging (HARDI) allows superior delineation of angular microstructures of brain white matter, and makes possible multiple-fiber modeling of each voxel for better characterization of brain connectivity. However, in the context of image registration, the question of how much information is needed for satisfactory alignment remains unanswered. Low order representation of the diffusivity information is generally more robust than the higher order representation, but the latter gives more information for correct fiber tract alignment. However, higher order representation, when naïvely utilized, might not necessarily be conducive to improving registration accuracy since similar structures with significant orientation differences prior to proper alignment might be mistakenly taken as non-matching structures. We propose in this paper a hierarchical spherical harmonics based registration algorithm which utilizes the wealth of information provided by HARDI in a more principled means. The image volumes are first registered using robust, relatively direction invariant features derived from the diffusion-attenuation profile, and their alignment is then refined using spherical harmonic (SH) representation of gradually increasing order. This progression of SH representation from non-directional, single-directional to multi-directional representation provides a systematic means of extracting directional information from the HARDI data. Experimental results show a significant increase in registration accuracy over a state-of-the-art DTI registration algorithm.

1 Introduction

The shortcoming of Diffusion Tensor Imaging (DTI) in resolving intra-voxel multiple fiber crossings has prompted great interest in developing more sophisticated models. Notably, Tuch et al. [1,2] introduced the High Angular Resolution Diffusion Imaging (HARDI) method, suggesting that the apparent diffusion coefficients could be evaluated along many different directions without fitting a global function to the data. The outcome is a diffusivity profile consisting of an angular distribution of apparent diffusivities, which allows a more complex representation of each voxel, and makes capturing multi-fiber information possible. This,

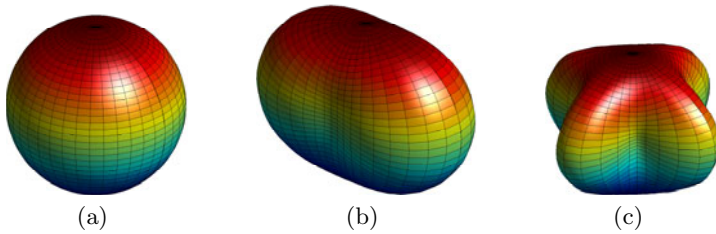


Fig. 1. (a) Zeroth order, (b) second order, and (c) fourth order SHs for representing isotropic, single-fiber and dual-fiber diffusivity profiles

however, presents new problems in the context of image registration. In particular, the question of how much information is actually needed for achieving satisfactory registration is still unanswered.

In view of the exciting insights into the brain HARDI can offer, there has been a recent flourish of HARDI registration algorithms. Fourth order tensors [3], along with a distance called the Hellinger distance, were employed by Barmoutis et al. [4] for registration of human hippocampi. Geng et al. [5] proposed a method which utilizes a spherical harmonic (SH) representation of the orientation distribution function (ODFs). Reorientation was performed directly on the SH coefficients, in a manner similar to the Finite Strain (FS) tensor reorientation technique proposed by Alexander et al. [6], by extracting rotation matrices from local Jacobians. Cheng et al. [7] took a multi-compartmental approach which was based on Gaussian mixtures. Reorientation was performed on the individual Gaussian components, each representing a major fiber direction, using an extension of the Preservation of Principal Directions (PPD) method [7]. Hong et al. performed registration on the $b = 0$ images and applied the estimated deformation field on the diffusion-weighted images with retransformation — taking into account rotation, scaling, and shearing effects of the spatial transformation — of the fiber orientation distribution. Bloy and Verma [8] computed the SH band energies as features for use with a Demons-based multi-channel registration algorithm for alignment of HARDI data.

For effective utilization of the wealth of information afforded by HARDI, we propose in this paper a hierarchical SHs based HARDI registration algorithm. SHs [9] of different orders have been shown to be capable of representing different diffusivity patterns [10]. Specifically, zeroth, second and fourth order SHs (see Fig. 1) have basis functions with shapes which are sphere-like, cigar-like and cross-like — ideal for representing voxels with isotropic, single-fiber, and dual-fiber diffusivity profiles, respectively. This property presents a natural way of hierarchically extracting information from the diffusivity profile. The key of our approach involves representing the diffusion-attenuation profile with increasing complexity to help progressively refine the registration. This effectively allows lower order, relatively orientation invariant, but more robust representations to guide the initial registration and higher order, directional, more precise representations to refine the alignment. This approach puts high and low order information in their

proper contexts and helps avoid mismatching of diffusion directions arising from large structural orientation differences. Registration is achieved by employing a forward-backward-consistent soft-correspondence matching scheme.

2 Diffusion-Attenuation Descriptors

2.1 Spherical Harmonic Representation

SHs, denoted as Y_l^m , with l denoting the order and m the phase factor, are a basis for complex functions on the unit sphere. Explicitly, they are given as:

$$Y_l^m(\theta, \phi) = \sqrt{\frac{2l+1}{4\pi} \frac{(l-m)!}{(l+m)!}} P_l^m(\cos(\theta)) e^{im\phi} \quad (1)$$

where (θ, ϕ) obeys the physics convention ($\theta \in [0, \pi]$, $\phi \in [0, 2\pi]$) and P_l^m is an associated Legendre polynomial. Since diffusion signals are real and antipodal symmetric, it is sufficient to utilize a real basis function set of even orders, i.e., for $l = 0, 2, 4, \dots, L$ and $m = -L, \dots, 0, \dots, L$:

$$Y_l^m = \begin{cases} \sqrt{2} \cdot \text{Re}(Y_l^m), & -L \leq m < 0 \\ Y_l^0, & m = 0 \\ \sqrt{2} \cdot \text{Im}(Y_l^m), & 0 < m \leq L \end{cases} \quad (2)$$

where $\text{Re}(Y_l^m)$ and $\text{Im}(Y_l^m)$ represent the real and imaginary parts of Y_l^m , respectively.

We denote $S(\mathbf{g})$ as the diffusion-attenuation signals at a finite set of points on a sphere, where \mathbf{g} is the diffusion encoding direction in a pulsed-gradient spin-echo experiment. As a spherical function, it can be approximated as a linear combination of a set of SH basis functions:

$$S(\mathbf{g}) = \sum_{l=0}^L \sum_{m=-l}^l y_l^m Y_l^m(\mathbf{g}). \quad (3)$$

Order L determines the complexity of the representation. A higher value for L will bring the representation closer to the original signal and will hence extract more directional information [10]. The SH coefficients y_l^m are determined using a Laplace-Beltrami regularized least-squares estimator, as described in [11].

We note here that the diffusion-attenuation profile $S(\mathbf{g})$ has a shape which is different compared to the diffusivity profile used in [9,10] (see [11] for examples). For example, a voxel encoding a single fiber direction will have an oblate shape in contrary to the typical prolate shape of the diffusivity profile. However, one can still sufficiently represent the single-fiber-direction voxel by SHs up to the second order. The same goes for voxels with fiber crossings. SH representation of $S(\mathbf{g})$ was in fact used in [12,11] for computing the ODFs. Funk-Radon transform, working in tandem with Funk-Hecke theorem [11], allows us to obtain the ODF

by using scaled versions of the SH coefficients [11], i.e., $2\pi P_l(0)y_l^m$, where $P_l(x)$ is the Legendre polynomial of degree l . That is, the ODF given by $S(\mathbf{g})$ is:

$$\mathcal{G}[S](\mathbf{g}) = \sum_{l=0}^L \sum_{m=-l}^l 2\pi P_l(0)y_l^m Y_l^m(\mathbf{g}). \quad (4)$$

2.2 Statistical Descriptors and Edge Maps

We incorporate, in addition to SHs, the following statistical descriptors of the diffusion-attenuation profiles in the registration algorithm. The diffusion mean is computed over the unit sphere Ω :

$$\mu = \langle S(\mathbf{g}) \rangle = \frac{1}{4\pi} \int_{\mathbf{g} \in \Omega} S(\mathbf{g}) d\mathbf{g} = \frac{y_0^0}{\sqrt{4\pi}}, \quad (5)$$

characterizing the average diffusion magnitude. The diffusion deviation, which measures the deviation of the profile from its isotropic component, is defined as:

$$\rho^2 = \frac{\langle |S(\mathbf{g}) - \langle S(\mathbf{g}) \rangle|^2 \rangle}{\langle |S(\mathbf{g})|^2 \rangle} = \frac{\sum_{l=1}^L \sum_{m=-l}^l |y_l^m|^2}{\sum_{l=0}^{\infty} \sum_{m=-l}^l |y_l^m|^2}. \quad (6)$$

For better characterization of structural shapes, regional statistical descriptors consisting of regional diffusion mean:

$$\mu_{\mathcal{N}} = \langle \mu(\mathbf{z}) \rangle = \frac{1}{|\mathcal{N}|} \sum_{\mathbf{z} \in \mathcal{N}} \mu(\mathbf{z}) \quad (7)$$

and regional diffusion deviation:

$$\rho_{\mathcal{N}}^2 = \langle \sigma(\mathbf{z}) \rangle = \frac{\sum_{\mathbf{z} \in \mathcal{N}} |\mu(\mathbf{z}) - \mu_{\mathcal{N}}|^2}{\sum_{\mathbf{z} \in \mathcal{N}} |\mu(\mathbf{z})|^2} \quad (8)$$

are computed for the neighborhood \mathcal{N} of each voxel. Although the above measures can be computed via the SH coefficients, considerable time can be saved by direct computation using $S(\mathbf{q})$. In addition to these descriptors, we applied a Canny edge detector on the μ and ρ maps to obtain edge information (denoted as \mathcal{H}_{μ} , \mathcal{H}_{ρ}) for guiding the alignment of tissue boundaries. Example statistical and edge maps are shown in Fig. 2.

2.3 Feature Vector and Similarity Measure

For each voxel at location \mathbf{x} , the SH coefficients and diffusion-attenuation statistical descriptors are grouped into a vector $\mathbf{a}(\mathbf{x}) = [\mathbf{a}_1(\mathbf{x}), \mathbf{a}_2(\mathbf{x})]$, with:

$$\mathbf{a}_1(\mathbf{x}) = [\mu(\mathbf{x}), \rho(\mathbf{x}), \mu_{\mathcal{N}}(\mathbf{x}), \rho_{\mathcal{N}}(\mathbf{x}), \mathcal{H}_{\mu}(\mathbf{x}), \mathcal{H}_{\rho}(\mathbf{x})], \quad \mathbf{a}_2(\mathbf{x}) = [\{w_l y_l^m(\mathbf{x})\}] \quad (9)$$

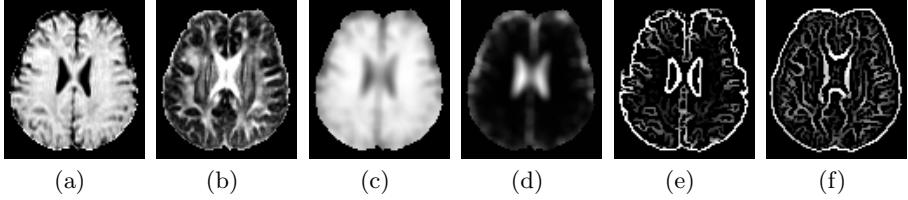


Fig. 2. Statistical and edge maps: (a) Mean, μ , (b) Deviation, ρ , (c) Regional mean, μ_N , (d) Regional deviation, ρ_N , (e) μ edge map, \mathcal{H}_μ and (f) ρ edge map, \mathcal{H}_ρ

where $\{w_l y_l^m(\mathbf{x})\}$ is the set of weighted SH coefficients computed up to order L . The weight of each order-band l is given by w_l ($w_0 = 1 \geq w_{l-2} \geq w_l \geq 0$). For our implementation, we set $w_2 = u(\alpha_2\tau)$ and $w_4 = u(\alpha_4\tau)$, where $u(\cdot)$ is a step function, for allowing the matching of single-fiber and dual-fiber information after $\alpha_2, \alpha_4 \in [0, 1]$ ($\alpha_2 < \alpha_4$) fractions of the total number of matching iterations, τ , respectively. This is so that progressively higher order representations can be employed to refine the registration. Normalizing the elements of $\mathbf{a}_1(\mathbf{x})$ to have a range of $[0, 1]$, the similarity measure can be defined as:

$$\eta(\mathbf{x}_T, \mathbf{x}_S) = \left\{ \Theta [\mathbf{a}_1(\mathbf{x}_T) - \mathbf{a}_1(\mathbf{x}_S)] \right\} \times \left\{ \frac{\mathbf{a}_2(\mathbf{x}_T) \cdot \mathbf{a}_2(\mathbf{x}_S)}{\|\mathbf{a}_2(\mathbf{x}_T)\| \times \|\mathbf{a}_2(\mathbf{x}_S)\|} \right\} \quad (10)$$

where $\Theta[\mathbf{a}] = \prod_k (1 - |a_k|)$, and \mathbf{x}_T and \mathbf{x}_S are specific voxels in the template image and the subject image, respectively. For robustness, we employ instead regional similarity measures:

$$\begin{aligned} \eta_{\mathcal{M}}(\mathbf{x}_T, \mathbf{x}_S) &= \frac{1}{|\mathcal{M}(\mathbf{x}_T)|} \sum_{\mathbf{z} \in \mathcal{M}(\mathbf{x}_T)} \eta(\mathbf{z}, \mathbf{x}_S + f(\mathbf{z}) - f(\mathbf{x}_T)) \\ \eta_{\mathcal{M}}(\mathbf{x}_S, \mathbf{x}_T) &= \frac{1}{|\mathcal{M}(\mathbf{x}_S)|} \sum_{\mathbf{z} \in \mathcal{M}(\mathbf{x}_S)} \eta(\mathbf{x}_T + f^{-1}(\mathbf{z}) - f^{-1}(\mathbf{x}_S), \mathbf{z}) \end{aligned} \quad (11)$$

which compare the similarity of the feature vectors in the neighborhood \mathcal{M} surrounding \mathbf{x}_T in the template image with that of \mathbf{x}_S in the subject image with consideration of the transformation f . Note that similarity measures in both directions are defined so that they can be employed for forward-backward consistent matching, described in the next section. The SH coefficients are re-estimated in each iteration of the registration to take into account the effect of the spatial transformation has on the diffusion-attenuation profile.

3 HARDI Registration

Registration of the HARD images can be achieved by minimizing the following cost function:

$$C(\mathbf{P}_T, \mathbf{P}_S, f) = \underbrace{C(\mathbf{P}_T, f) + C(\mathbf{P}_S, f)}_{\text{Matching}} + \underbrace{C(\mathbf{P}_T) + C(\mathbf{P}_S)}_{\text{Soft Correspondence}} + \underbrace{C(f)}_{\text{Smoothness}} \quad (12)$$

Matching: Voxel at \mathbf{x}_T and voxel at \mathbf{x}_S are deemed as a matching pair if they are close spatially and if their feature vectors show high similarity. Naturally, a voxel pair \mathbf{x}_T and \mathbf{x}_S satisfying these conditions will be given a higher probability value $p(\mathbf{x}_T, \mathbf{x}_S)$ in the cost function. We also enforce a symmetric matching mechanism [13] which avoids bias towards the template or the subject. The cost functions are defined as:

$$\begin{aligned} C(\mathbf{P}_T, f) &= \sum_{\mathbf{x}_T \in \mathcal{V}_T, \mathbf{x}_S \in \mathcal{V}_S} p_T(\mathbf{x}_T, \mathbf{x}_S) \left\{ \|f(\mathbf{x}_T) - \mathbf{x}_S\|^2 - \log [\eta_{\mathcal{M}}(\mathbf{x}_T, \mathbf{x}_S)] \right\} \\ C(\mathbf{P}_S, f) &= \sum_{\mathbf{x}_T \in \mathcal{V}_T, \mathbf{x}_S \in \mathcal{V}_S} p_S(\mathbf{x}_T, \mathbf{x}_S) \left\{ \|\mathbf{x}_T - f^{-1}(\mathbf{x}_S)\|^2 - \log [\eta_{\mathcal{M}}(\mathbf{x}_S, \mathbf{x}_T)] \right\} \end{aligned} \quad (13)$$

where $\mathbf{P}_T = \{p_T(\mathbf{x}_T, \mathbf{x}_S)\}$ and $\mathbf{P}_S = \{p_S(\mathbf{x}_T, \mathbf{x}_S)\}$. \mathcal{V}_T and \mathcal{V}_S represent the template and subject brain domains, respectively.

Soft Correspondence: Soft correspondence are permitted in the initial stages of the registration to allow robust matching based on multiple candidate points. Towards the end of the registration, more exact one-to-one correspondence is enforced. This is realized by energy terms:

$$\begin{aligned} C(\mathbf{P}_T) &= \gamma \sum_{\mathbf{x}_T \in \mathcal{V}_T, \mathbf{x}_S \in \mathcal{V}_S} p_T(\mathbf{x}_T, \mathbf{x}_S) \log(p_T(\mathbf{x}_T, \mathbf{x}_S)), \\ C(\mathbf{P}_S) &= \gamma \sum_{\mathbf{x}_T \in \mathcal{V}_T, \mathbf{x}_S \in \mathcal{V}_S} p_S(\mathbf{x}_T, \mathbf{x}_S) \log(p_S(\mathbf{x}_T, \mathbf{x}_S)). \end{aligned} \quad (14)$$

where \mathcal{V}_T and \mathcal{V}_S represent the template and subject brain domains, respectively. Parameters γ controls the degree of fuzziness of the matching. It has initially high values, encouraging fuzzy matching, and later progressively lower values, which enforce exact matching.

Transformation Regularization: Mapping f is required to be smooth for preserving a biologically sensible topology. This is enforced by energy term: $E(f) = \beta \|\mathcal{L}f\|^2$. \mathcal{L} is an operator which aids in measuring the bending energy. β is a weighting factor which is decreased throughout the registration to allow f to model deformation of increasing complexity.

Optimization: The cost function (12) can be minimized by alternating between correspondence matching and dense transformation estimation [14, 15]. We first fix f and solve for \mathbf{P}_T and \mathbf{P}_S by letting $\partial C(\mathbf{P}_T, \mathbf{P}_S, f) / \partial p_T(\mathbf{x}_T, \mathbf{x}_S) = 0$ and $\partial C(\mathbf{P}_T, \mathbf{P}_S, f) / \partial p_S(\mathbf{x}_T, \mathbf{x}_S) = 0$. We then fix \mathbf{P}_T and \mathbf{P}_S , and solve for f using thin-plate splines (TPS) [16, 17].

Retransformation of Spherical Harmonics: Barmpoutis et al. [4] noted the limitations of reorientation of diffusivity functions and proposed instead to employ a full affine *retransformation*. In our case, although a SH reorientation strategy was proposed by Geng et al. [5], we have opted accuracy over speed or convenience by re-estimating the SH coefficients in each iteration of registration. That is, for a local transform \mathbf{F} , we tilt the gradient directions by $\mathbf{g}' = \mathbf{F}\mathbf{g} / \|\mathbf{F}\mathbf{g}\|$ (see Fig. 3), and compute a new set of SH coefficients $\{y_l^m\}$.

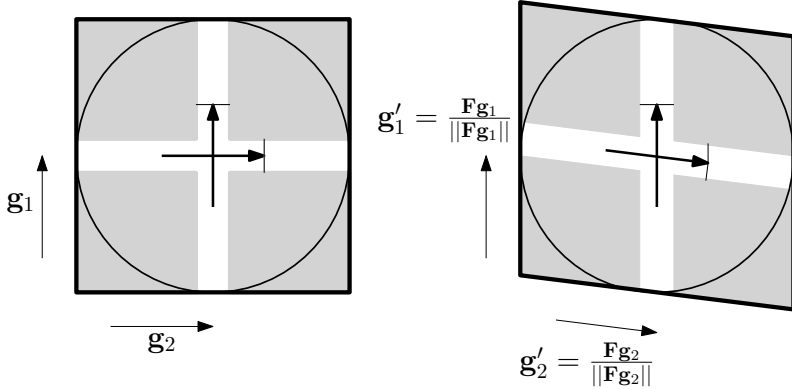


Fig. 3. Retransformation of diffusion-attenuation profile. Each diffusion direction \mathbf{g} is transformed by the local transformation matrix \mathbf{F} to become $\mathbf{g}'_i = \mathbf{F}\mathbf{g}_i / \|\mathbf{F}\mathbf{g}_i\|$.

4 Experimental Results

Six adult subjects were scanned using an EPI sequence with diffusion gradients applied in 120 non-collinear directions. 80 contiguous slices with slice thickness of 2mm covered a field of view (FOV) of $256 \times 256\text{mm}^2$ with an isotropic voxel size of 2mm. Out of the 6 HARD images, one was selected as the template onto which the rest were registered. To demonstrate the effectiveness of the proposed method over DTI-based registration, we employed a state-of-the-art DTI registration algorithm [15, 14] for comparison. We reconstructed the diffusion tensors (DTs) of the diffusion-weighted images and register the DT images using the above-mentioned algorithm. The estimated deformation fields were then used to warp and retransform the respective HARD images. We have also compared our results with FLIRT [18] applied on the deviation maps (see Fig. 2(b)) for affine registration. The orientation consistency (OC) was assessed using the voxel-wise scalar product of the principal orientation direction, \mathbf{g}_{PD} , of each voxel in an aligned image with respect to the template:

$$\text{OC} = \sum_{\mathbf{x} \in \mathcal{V}_{\text{T}}} |\mathbf{g}_{\text{PD}}^{\text{subject}}(\mathbf{x}) \cdot \mathbf{g}_{\text{PD}}^{\text{template}}(\mathbf{x})|. \quad (15)$$

The absolute value was taken since diffusion directions are antipodal symmetric. The principal directions were estimated by a 1082 point even sampling of the orientation distribution functions (ODFs) using Camino [19]. Comparison was made only for voxel showing significant anisotropy (voxels with deviation value $\rho > 0.1$). Compared with DTI-based registration, we found an overall improvement in white-matter orientational consistency of 3.02% ($p < 0.05$). Compared with affine registration, an improvement of 7.39% ($p < 0.001$) was achieved. Results for each individual subject, shown in Fig. 4, indicate that the proposed method gives consistent improvement across subjects.

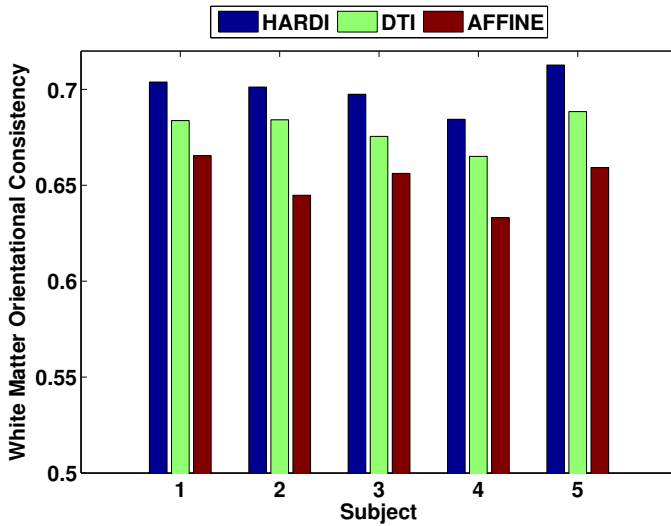


Fig. 4. White matter orientational consistency for individual subjects

5 Conclusion

We have proposed a HARDI registration algorithm which, in a principled manner, extracts orientation information from the diffusion-attenuation profile. The useful property of spherical harmonics in representing different levels of orientation complexity of the diffusion pattern is utilized to progressively provide the registration process with increasing levels of information for alignment refinement. Experimental results indicate better registration accuracy than DTI-based registration algorithm, further validating the fact that the information given by HARDI can be utilized to improve structural alignment.

Acknowledgment

This work was supported in part by grants EB006733, EB008760, EB008374, EB009634, and MH088520.

References

1. Tuch, D.S., Weisskoff, R.M., Belliveau, J.W., Wedeen, V.J.: High angular resolution diffusion imaging of the human brain. In: ISMRM 1999 (1999)
2. Tuch, D.: Q-ball imaging. *Magnetic Resonance in Medicine* 52(6), 1358–1372 (2004)
3. Bampoutis, A., Hwang, M.S., Howland, D., Forder, J.R., Vemuri, B.C.: Regularized positive-definite fourth order tensor field estimation from DW-MRI. *NeuroImage* 45, 153–162 (2009)

4. Barmpoutis, A., Vemuri, B.C., Forder, J.R.: Registration of high angular resolution diffusion MRI images using 4th order tensors. In: Ayache, N., Ourselin, S., Maeder, A. (eds.) MICCAI 2007, Part I. LNCS, vol. 4791, pp. 908–915. Springer, Heidelberg (2007)
5. Geng, X., Ross, J.T., Zhan, W., Gu, H., Chao, Y.P., Lin, C.P., Christensen, G.E., Schuff, N., Yang, Y.: Diffusion MRI registration using orientation distribution functions. In: Prince, J.L., Pham, D.L., Myers, K.J. (eds.) IPMI 2009. LNCS, vol. 5636, pp. 627–637. Springer, Heidelberg (2009)
6. Alexander, D.C., Pierpaoli, C., Basser, P.J., Gee, J.C.: Spatial transformations of diffusion tensor magnetic resonance images. *IEEE Transactions on Medical Imaging* 20(11), 1131–1139 (2001)
7. Cheng, G., Vemuri, B.C., Carney, P.R., Mareci, T.H.: Non-rigid registration of high angular resolution diffusion images represented by Gaussian mixture fields. In: Yang, G.-Z., Hawkes, D., Rueckert, D., Noble, A., Taylor, C. (eds.) MICCAI 2009. LNCS, vol. 5761, pp. 190–197. Springer, Heidelberg (2009)
8. Bloy, L., Verma, R.: Demons registration of high angular resolution diffusion images. In: Proceedings of IEEE International Symposium on Biomedical Imaging (ISBI 2010), pp. 1013–1016 (2010)
9. Alexander, D., Barker, G., Arridge, S.: Detection and modeling of non-Gaussian apparent diffusion coefficient profiles in human brain data. *Magnetic Resonance in Medicine* 48, 331–340 (2002)
10. Frank, L.R.: Characterization of anisotropy in high angular resolution diffusion-weighted MRI. *Magnetic Resonance in Medicine* 47, 1083–1099 (2002)
11. Descoteaux, M., Angelino, E., Fitzgibbons, S., Deriche, R.: Regularized, fast, and robust analytical q-ball imaging. *Magnetic Resonance in Medicine* 58, 497–510 (2007)
12. Hess, C.P., Mukherjee, P., Han, E.T., Xu, D., Vigneron, D.B.: Q-ball reconstruction of multimodel fiber orientations using the spherical harmonic basis. *Magnetic Resonance in Medicine* 56, 104–117 (2006)
13. Christensen, G.E.: Consistent linear-elastic transformations for image matching. In: *Information Processing in Medical Imaging*, pp. 224–237 (1999)
14. Yap, P.T., Wu, G., Zhu, H., Lin, W., Shen, D.: Fast Tensor Image Morphing for Elastic Registration. In: Yang, G.-Z., Hawkes, D., Rueckert, D., Noble, A., Taylor, C. (eds.) MICCAI 2009. LNCS, vol. 5761, pp. 721–729. Springer, Heidelberg (2009)
15. Yap, P.T., Wu, G., Zhu, H., Lin, W., Shen, D.: F-TIMER: Fast Tensor Image Morphing for Elastic Registration. *IEEE Transactions on Medical Imaging* 29, 1192–1203 (2010)
16. Bookstein, F.L.: Principal warps: Thin-plate splines and the decomposition of deformations. *IEEE Transactions on Pattern Analysis and Machine Intelligence* 11(6), 567–585 (1989)
17. Chui, H., Rangarajan, A.: A new point matching algorithm for non-rigid registration. *Computer Vision and Image Understanding* 89(2-3), 114–141 (2003)
18. Smith, S.M., Jenkinson, M., Woolrich, M.W., Beckmann, C.F., Behrens, T.E., Johansen-Berg, H., Bannister, P.R., Luca, M.D., Drobnjak, I., Flitney, D.E., Niazy, R.K., Saunders, J., Vickers, J., Zhang, Y., Stefano, N.D., Brady, J.M., Matthews, P.M.: Advances in functional and structural MR image analysis and implementation as fsl. *NeuroImage* (23), S208–S219 (2004)
19. Cook, P.A., Bai, Y., Nedjati-Gilani, S., Seunarine, K.K., Hall, M.G., Parker, G.J., Alexander, D.C.: Camino: Open-source diffusion-MRI reconstruction and processing. In: 14th Scientific Meeting of the International Society for Magnetic Resonance in Medicine, vol. 2759 (2006)